

Delay Time (δt) and Polarization Direction (ϕ) Analysis Based on Shear Wave Splitting (SWS) Method

Widya Utama^{a,*}, Sherly Ardhya Garini^a, Valda Anggita Kurnia^a, Wien Lestari^a, Dwa Desa Warnana^a

^a Geophysical Engineering Department, Institut Teknologi Sepuluh Nopember (ITS), Surabaya, 60111, Indonesia

Corresponding author: *widya@geofisika.its.ac.id

Abstract— The information of dominant polarization direction and the mapping of fracture intensity are among the most important informations during the monitoring of geothermal field reservoir evaluation, as an effort to develop geothermal energy production. The appearance of geothermal reservoir fractures caused by fluid injection and the production activity resulting in the decreased pore pressure and appearance of open weak zone. The micro-earthquake activity around the area can represent these fractures that appear in the geothermal reservoir. Shear Wave Splitting (SWS) analysis can be done based on the polarization of S wave through the anisotropy medium recorded by seismograph. There are two parameters related to Shear Wave Splitting: the polarization direction (ϕ) related to the micro fracture direction with its delay time (δt), showing the fractures density and its permeability area. The result of Shear Wave Splitting Analysis of the field X geothermal shows that two dominant polarization directions are NW-SE and NE-SW. It is caused by the fractures around the X field geothermal with similar fractures direction, and it is compatible with the distribution micro-earthquake hypocenter of the previous study. Based on the map of fractures intensity, the value range shows a relatively dense intensity value around 6.6 – 8.0 ms/km. The high value of intensity fractures indicates a high value of anisotropy around the area, and it is also confirming the presumption of the high permeability potential of the X geothermal field.

Keywords— Delay time; geothermal; polarization direction; shear wave splitting.

Manuscript received 4 Sep. 2020; revised 13 Apr. 2021; accepted 29 May 2021. Date of publication 31 Oct. 2022.
IJASEIT is licensed under a Creative Commons Attribution-Share Alike 4.0 International License.



I. INTRODUCTION

The study of earthquakes in a geothermal system mainly focused on the micro-earthquake [1]. Investigation of micro-earthquake with magnitude ≤ 3 RS on the active tectonic plate zone and volcanic areas have shown hydrothermal convection systems characterized by micro-earthquake activity [2]. The appearance of fractures on the geothermal reservoir is one of the main causes of micro-earthquakes in the geothermal system [3]. These fractures occur due to the fluid injection and the production activity resulting in a decreased pore pressure, appearance of the weak open zone, and the contiguity of cold water with hot rocks [3]–[5]. Information about the fractures in the geothermal field is needed for the development of geothermal energy production [1]. Shear Wave Splitting is one of the methods used to identify the direction and structure of fractures [6], [7].

Shear Wave Splitting (SWS) analysis is one of the geophysics analyses of waves that can be used to analyze the anisotropy of the medium layer of the earth [8], [9]. Shear Wave Splitting analysis has been widely used to study seismic

to identify the anisotropy inside the earth [10], [11]. Shear Wave Splitting (SWS) is a secondary (S) wave phenomenon, which has been polarized while entering an anisotropy medium [12]. When the S wave gets into the anisotropy medium, the wave's polarization will split in two perpendicularly, known as S_{fast} and S_{slow} [9]. S_{fast} wave will be parallel to fracture correlating with the fracture's strike, while S_{slow} will be parallel with the direction of the fracture [13]. By using the Shear Wave Splitting method, the parameters of polarization (ϕ) and delay time (δt) can be identified [9]. The direction of the S wave polarization (ϕ) related to the direction of the microfracture, while the delay time (δt) of the two waves (S_{fast} and S_{slow}) shows the density of the fracture and the permeability area [14].

II. MATERIAL AND METHOD

This research is using secondary data which belongs to the geothermal field X company. Concerning the company as the owner, the confidential data will not be displayed in this study (the coordinate point with specific geographic information of the area).

RAW data (waveform) recorded at the research location (geothermal field X) is a 3-component seismogram, consist of one vertical component (Z) and two horizontal components (N-S and E-W). This study's waveform selection to be analyzed and processed refers to the distribution of micro-earthquake hypocenter locations determined using the Geiger method carried out in a similar research area [15]. S wave polarization phenomenon can be analyzed by observing the horizontal component N-S and horizontal component E-W, where one component will show the appearance of S fast wave (S_{fast}) and S slow-wave (S_{slow}) in the other component [16]. This time differences will result in delay time (δt) data [17].

This research only uses the seismograms recorded from four seismic stations in the study area, namely stations with the initials ULI, ZTO, BUA, and BRK, as shown in Fig. 1. Seismogram data, especially two horizontal components (N-S and E-W) of secondary (S) waves, are the primary data, which are processed using the particle motion method, and then analyzed using Shear Wave Splitting (SWS) method.

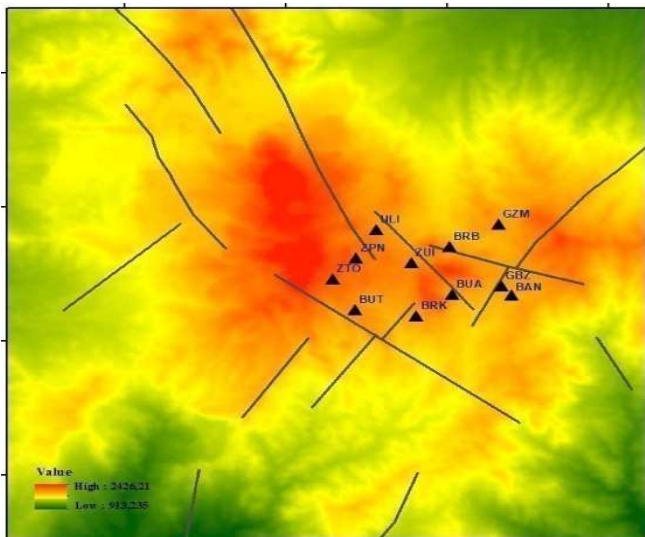


Fig. 1 The position of the seismic station on geothermal field X

A. Event Selection and Wave Phase Picking

Wave phase picking includes determining the arrival time, measuring, and determining the types to be used to determine and classify the location of a seismic event [18]. The following are the steps performed in manual phase picking:

- Clear phase identification of unfiltered traces (if applicable).
- Identification of primary wave phase (P) in the vertical component (Z) and secondary wave phase (S) to the horizontal component (N-S and E-W). The P wave comes earlier while the S wave comes later with a larger amplitude value.
- Labelling the P and S phases at the first break of the S wave determination from particle motion (vertical component (Z)) and the horizontal component (N-S)).

B. Filtering

Analyzing can be done by seeing each component or by using the frequency limit with the largest amplitude [19]. The next step is filtering based on the frequency limit with a band-pass filter [20]. Micro-earthquake data is being carried out

from the frequency spectrum and the spectrogram to determine the frequency width for the filtering process [21], [22]. Aside from that, spectrogram analysis is also needed to identify the variation of harmonic signal frequency towards the time [23]. This aims to determine the frequency limit, which will be used in the filtering process [19], [23]. The filtering uses the Butterworth band-pass filter because it is specialized for the filtering process (band-pass) [24], [25].

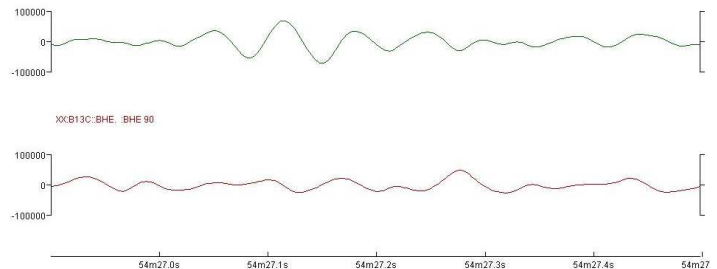


Fig. 2 The result of microseismic event recording of 3 components that have been sampled for 5 seconds before the filtering process

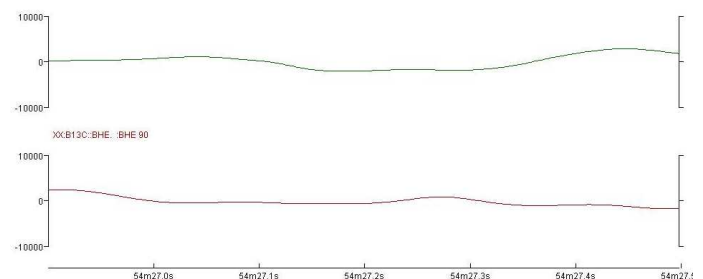


Fig. 3 The result of micro seismic event recording of 3 components that have been sampled for 5 seconds after band-pass filtering process

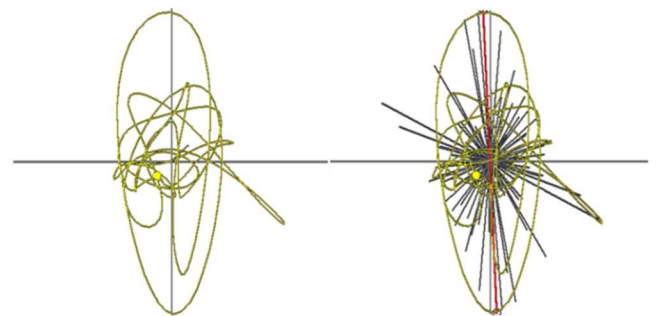


Fig. 4 Particle motion cutting wave from horizontal component N-S and E-W for 5 seconds from ZTO station before the filtering process

Fig. 2 is the result of wave recording before the filtering process. Meanwhile, Fig. 3 shows wave recording after the filtering process with a frequency limit between 8–10 Hz. The determination of frequency limit is based on the amplitude peak, estimating the original signal to be at that frequency. The predetermined frequency limit will then be used in the next step, which is the filtering stage.

There is something in common for the result of particle motion before and after being filtered. Both have a movement that forms a decreasing polarization direction towards the center of the axis point [26], [27]. It is marked that the direction of the particles indicates one particular direction continually without any interruption, as shown in Fig. 4 and Fig. 5. If other events occur in one movement, the direction of

the movement itself will be in the form of a big circle, then decreases and then return to the big circle. In other words, it is not continuous from the rotation of the decreasing magnitude.

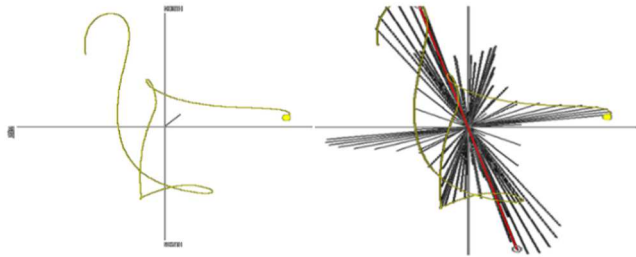


Fig. 5 Particle motion cutting wave from the horizontal component N-S and E-W for 5 seconds from ZTO station after filtering process

C. Parameter Shear Wave Splitting (SWS)

Secondary waves (S) passing through the medium with vertically oriented fractures will result in the separation of SH and SV components, with SV coming faster (earlier) than SH, which comes slower. In other words, S waves that propagate perpendicularly with the fracture will come slower, while the S wave that is parallel to the fracture will come faster [28]. With further development, delay time (δt) will be bigger if the S wave propagates perpendicularly to the fracture, and it will be smaller if it propagates parallel or in line with the fracture [29].

Shear Wave Splitting (SWS) analysis is a recording phenomenon of the secondary wave (S) on the horizontal components of microseismical data, namely N-S and E-W marked with S_{fast} recording and then followed by S_{slow} wave. The polarization phenomenon of S wave can be analyzed by observing the horizontal component of N-S and E-W shown in Fig. 6. One of the components will show the appearance of S_{fast} and S_{slow} waves on the seismic wave component. The time difference of the arrival between S wave parameter will produce $d(\delta t)$ data [30]. Polarization angle measurement is done by observing the plot diagram of particle motion horizontal components of S wave. In Fig. 7 the particle motion at the S wave's beginning is the S_{fast} wave's particle motion. And then, followed by a sudden perpendicular motion with the previous S_{fast} particle motion, this motion belongs to the S wave, which has been polarized and known as S_{slow} . The S_{fast} motion is forming a north-facing direction. To get the azimuth value, it is assumed that S_{fast} direction is heading towards the north [31].

After obtaining the polarization angle and delay time of the S wave passing through a fracture, a ray path calculation can be performed from the location of the hypocenter point. Raypath is the average length of one hypocenter to the micro-earthquakes recording station and is considered a straight line [32], [33]. Then, the previously known delay time (δt) is divided by the previously calculated ray path value to determine the fracture intensity value.

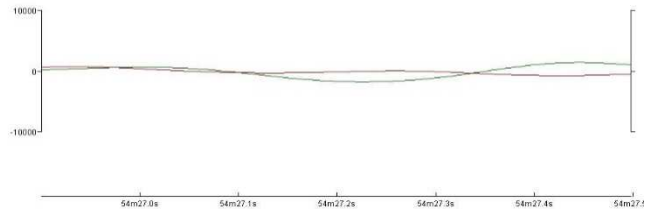


Fig. 6 Shear Wave Splitting Phenomenon from the horizontal component N-S and E-W of ZTO station

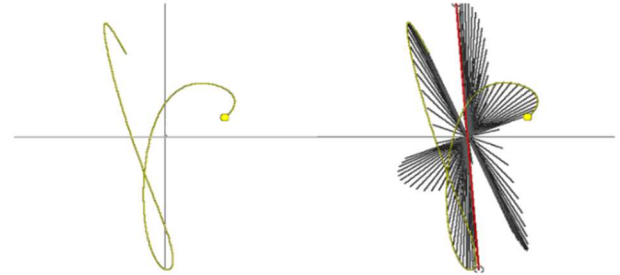


Fig. 7 Particle motion cutting wave from horizontal component N-S and E-W from ZTO station

The distribution of the epicenter points location used in this study (check Fig. 8) is the distribution of the hypocenter location of micro-earthquakes determined using the Geiger method, which was carried out in a similar research area.

The research result in 73 hypocenter coordinates using 11 seismic stations in the same research area. Therefore, after the processing and calculation stages have been carried out, the dominant direction interpretation of micro-fractures at one station to another can be carried out.

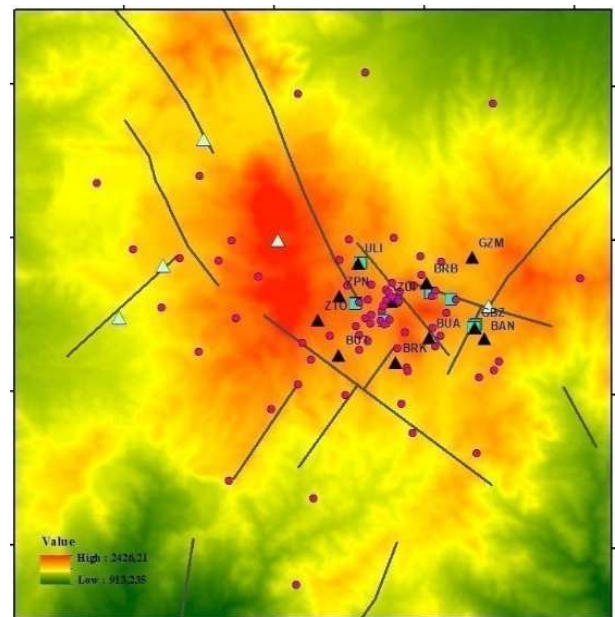


Fig. 8 Distribution of micro epicenter earthquakes result using Geiger method

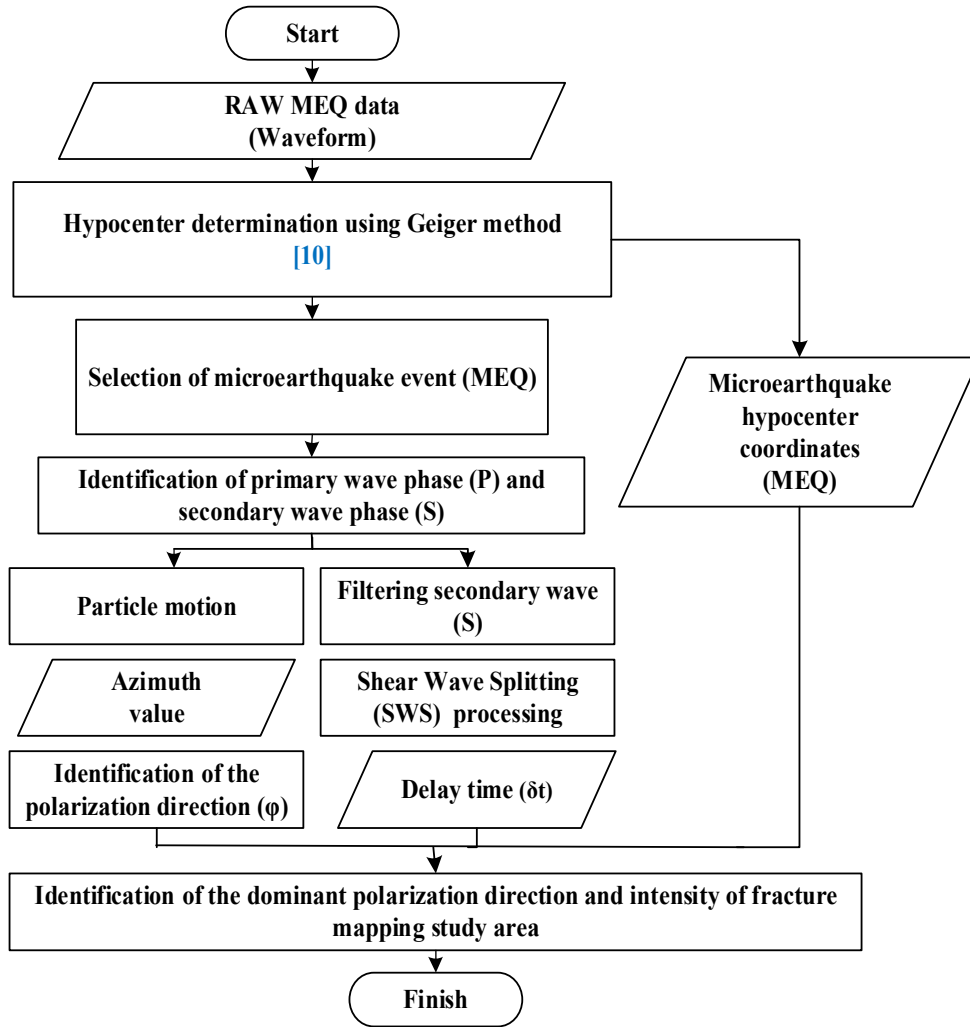


Fig. 9 Research Flowchart

III. RESULT AND DISCUSSION

Based on the result data using Shear Wave Splitting (SWS) method, two parameters are obtained, which are the direction of polarization (φ) related to the dominant direction of the micro fracture, and the delay time (δt) which can interpret the anisotropy medium (micro fracture intensity) passed by the seismic wave as they propagate. Polarization direction and delay time can be analysed based on the observation of particle motion through a particle motion diagram [17].

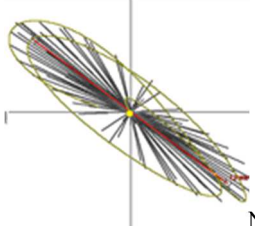
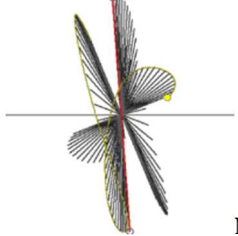
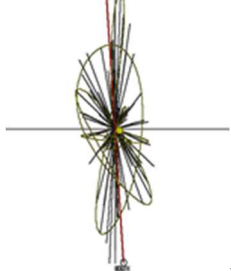
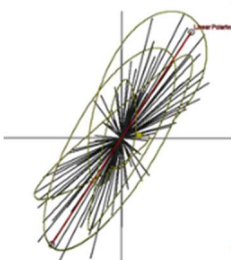
A. Polarization Direction (φ)

Identification of the dominant direction of the micro fracture can be obtained from the observation result of polarization direction (φ) S_{fast} wave at each seismic recording station. The happening polarization shows by the appearance of the wave, which propagates, perpendicularly to the direction of the particle motion. S_{fast} wave direction rotates based on the angle of the movement of the particles. If the S_{fast} wave starts moving in the north direction, the next is determined as the polarization direction. Each earthquake event will provide a certain polarization direction, and the diversity of directions shown in the motion particle diagram for each station and each event shows that the seismic wave propagation medium

is an anisotropy medium. Polarization direction from each event will be accumulated by seismic station; each station has its dominant direction of polarization value. Based on the particle motion direction from each event recorded by each station shown in Table 1, the S_{fast} polarization data obtained as follows: The direction of station recording shows various dominant directions with a quite consistent value. First, ULI seismic station shows the polarization value (φ) N 127° E. Then, ZTO station shows polarization value (φ) N 176° E, BUA station shows polarization value (φ) N 106° E, and BRK station shows polarization value (φ) N 149° E.

Even though the polarization direction on each station shows a dominant value, but the recorded direction is full of diversity, showing that the seismic wave propagation area is an anisotropy area. The polarization direction is correlated with the data of the fault, and it is being correlated with the seismic station position, which records the micro-earthquake on the geothermal field X. In Table 1, the result of the particle motion process shows polarization direction based on the depth. Table 1 shows the result of the polarization direction for the depth of 0 to -2000 m on each station (was cut) vertically. Based on Table 1, it can be concluded that the polarization direction gained from each station has an angle directed towards the North and East.

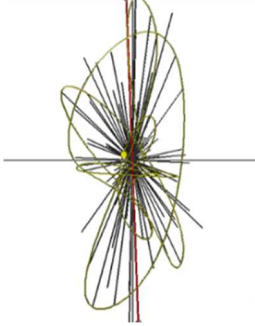
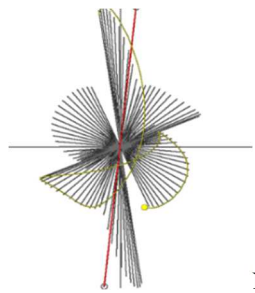
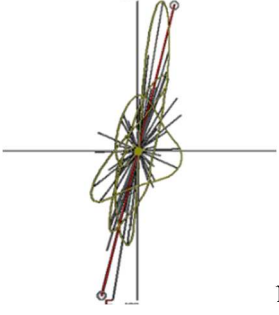
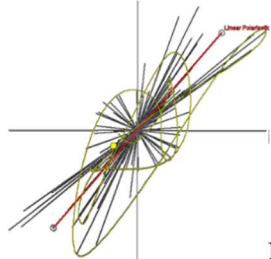
TABLE I
POLARIZATION DIRECTION OF EACH SEISMIC STATION (ULI, ZTO, BUA AND BRK) IN THE LINEAR POLARIZATION DIAGRAM AT THE DEPTH OF -2000 TO 0 METER

Station	Polarization Direction (ϕ)
ULI	 N 127° E
ZTO	 N 176° E
BUA	 N 106° E
BRK	 N 149° E

The previous research [15] determined the distribution of micro-earthquake hypocenter results using the Geiger method, at a depth of 2000 to -2000 m spread around the seismic station. Thus, slicing was carried out in the depth of 2000 to 0 m and 0 to -2000 m. In the depth of 0 to 2000 m shown in Table 2, deflection appears at each recording station on each captured layer. The ULI station within depth of -2000 to 0 m has the polarization value of N 127° E, and deflection value N 173° E appears at a depth of 0 to 2000 m. In ZTO station with the depth of -2000 to 0 m has the polarization value of N 176° E while at a depth of 0 to 2000m has the polarization direction value of N 194° E. For BUA station in the depth of -2000 to 0 m shows the polarization direction of N 106° E while at a depth of 0 to 2000 m has the polarization value of N 173° E. Meanwhile, BRK station has a polarization direction value of N 149° E in the depth of -2000 to 0 m, and in the depth of 0 to 2000 m, it has N 137° E value. From the result of the research, it can be assumed that the polarization direction of the microseismic event is affected by the appearance of the hypocenter point parallel to the fracture direction. Based on that result, it can also be concluded that

the direction of the wave particles movement for each event has gone through some changes. It is because the waves propagate from the hypocenter of the micro-earthquake through the anisotropic towards the seismic recording station.

TABLE II
THE POLARIZATION DIRECTION OF EACH SEISMIC STATION (ULI, ZTO, BUA AND BRK) IN THE LINEAR POLARISAZATION DIAGRAM IN THE DEPTH OF 0 TO 2000 METER

Station	Polarization Direction (ϕ)
ULI	 N 173° E
ZTO	 N 194° E
BUA	 N 104.15° E
BRK	 N 137° E

The research results show that there are two dominant polarization directions: NW – SE and NE – SW. The polarization direction of the recording station is integrated with the presence of local faults below the surface. When the direction of the polarization is parallel to the local fault, the recorded anisotropic area is controlled by the surrounding structure near the recorded event. It can be assumed that the

continuous fractures from the bottom to the surface have a parallel position to the active fault.

B. Fracture Intensity

The thickness of the anisotropy medium or the intensity of the micro-fracture can be shown by the delay time between S_{fast} and S_{slow} waves. Delay time is the difference between the arrival time of S_{fast} and S_{slow} waves passing through the anisotropic medium recorded by seismogram at the seismic recording station. The delay time value for shear wave splitting depends on the material's length and the fracture's intensity in the anisotropy medium below the surface. It is because the greater the anisotropy value, the greater the value of the shear wave splitting delay time parameter. Moreover, vice versa, the smaller anisotropy value, the delay time parameter value of the shear-splitting wave will be smaller too.

In order to compare the delay time from different sources correctly, normalization is needed between the values of delay time with the length of raypath to recognize the fracture intensity. Raypath value is the average length from one hypocenter to the recording station, which records the micro-earthquake event that is considered straight. In this research, hypocenter location coordinates is determined using the previous study [15]. After the value of the delay time and raypath length obtained, then the value of fracture intensity can be identified. The result of dividing the delay time with raypath is a normalization step to obtain the fracture intensity value. Based on the processing results, the average value of the delay time and the average length from one hypocenter to the station (raypath) and the fracture intensity at each earthquake recording station is obtained. Therefore, based on the result of this calculation, it can be interpreted in Fig. 10, which is the delay time contour map, Fig. 11 as the raypath contour map, and Fig. 12 as the contour map of the fracture intensity in the research area.

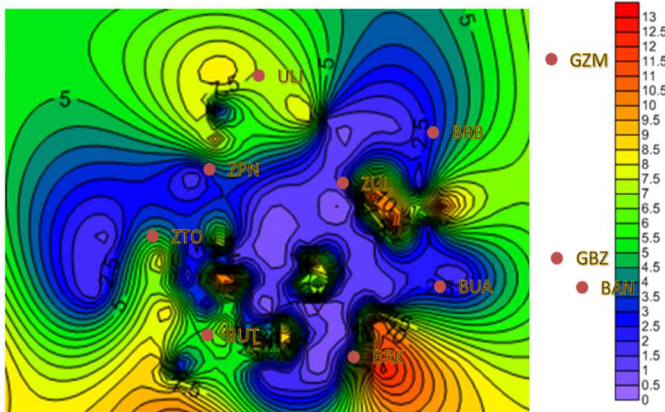


Fig. 10 Delay time contour map for Geothermal Field X

The delay time contour map in each earthquake recording station represents the spread of the high delay time value around the area of ULI, BUT, GZM, and BAN station around the research area. Meanwhile, the lower value of delay time spread around the other station around the research area: ZPN, ZTO, ZUI, BRB, BUA, and BRK station.

As a whole, delay time values range from 2 – 9.5 ms as shown in Fig. 10, the highest value is in the western area of the research location, while the east-south area shows a

relatively lower value. The existence of the delay time value still could not indicate the fracture thickness in the anisotropy medium in which the wave propagates. The track of raypath contour map shown in Fig. 11 shows that the low distribution of raypath values occurs in ZPN, ZTO, ZUI, BRB, BRK, BUA, and BRK station.

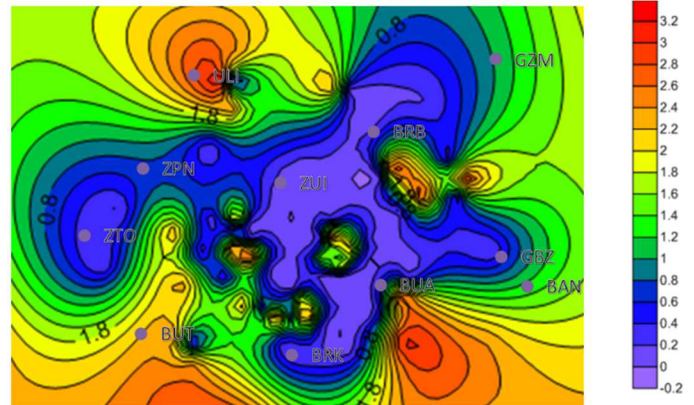


Fig. 11 Raypath Contour Map for Geothermal Field X

Meanwhile, the higher raypath value spread around the area of ULI, BUT, BAN, and GZM station. Lower raypath value around the area of southeast research location indicates the number of earthquakes happen around that area, resulting in a shorter wave's propagation trajectory. On the other hand, the opposite result happens in the western area of research location. It is because the raypath value is getting bigger due to the bigger distance of epicenter value. The contour map of fracture intensity provides information regarding the thickness of the fracture, and the fracture intensity can be identified after the delay time distribution has been normalized using the length of the wave path (raypath).

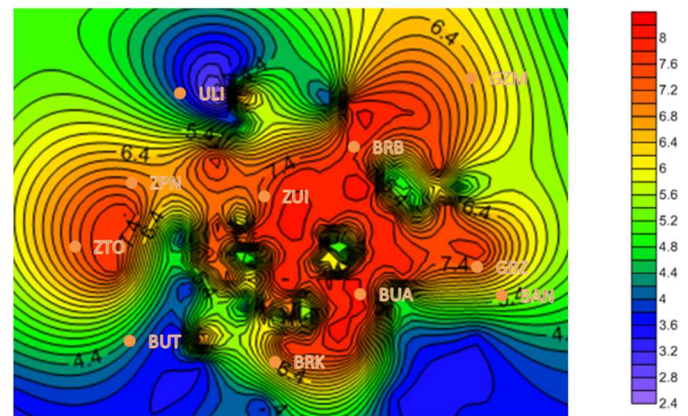


Fig. 12 Fracture Intensity Contour Map of Geothermal Field X

Based on the fracture intensity contour map in Fig. 12, the fracture intensity with relative dense values in the range of 6.6 – 8.0 ms/km. The higher intensity fracture values can be found in the southern area of the research location, which is in ZTO, ZPN, ZUI, BRK, and BRB stations. Meanwhile, the lower value of fracture intensity can be found in the western and eastern parts of the research area, which are ULI, GZM, BAN, GBZ, and BUT stations. The high value of fracture intensity alongside the high intensity of the structure strengthens the suspicion of high permeability potential in the area.

IV. CONCLUSIONS

There are two dominant directions of shear wave splitting polarization at each station: NW – SE and NE– SW. Faults cause this around the geothermal field with similar fault direction, which is also under the distribution of micro-earthquake hypocenter locations in the previous studies.

The contour map of the fracture intensity shows a relatively dense range of fracture intensity with values ranging from 6.6 – 8.0 ms/km. The distribution of high fracture intensity values can be found in the southern area of the research location, which is ZTO, ZPN, ZUI, BRK, and BRB stations. Meanwhile, low fracture intensity values distribution can be found in the western and eastern parts of the research location, which are ULI, GZM, BAN, GBZ, and BUT station. High values of fracture intensity interpret high anisotropy in that area, which enhances the suspicion that there is a high potential of permeability in geothermal field X.

ACKNOWLEDGMENT

We thank PT Geo Dipa Energi (Persero) for permission to use the data in this research.

REFERENCES

- [1] M. R. Maulana, M. S. Rosid, Farhan, and C. Iskandar, "Identification of Fracture Density and Orientation at ' R ' Geothermal Field Using Shear Wave Splitting Microearthquake Method Identification of Fracture Density and Orientation at " R " Geothermal Field Using Shear Wave Splitting Microearthquake Method," 2019, doi: 10.1088/1742-6596/1351/1/012050.
- [2] W. I. Sevilla, L. A. Jumawan, C. J. Clarito, M. A. Quintia, A. A. Domingiano, and R. U. Solidum, "Improved 1D velocity model and deep long-period earthquakes in Kanlaon Volcano, Philippines: Implications for its magmatic system," *J. Volcanol. Geotherm. Res.*, vol. 393, no. 106793, 2020, doi: 10.1016/j.jvolgeores.2020.106793.
- [3] D. Liotta and A. Brogi, "Pliocene-Quaternary fault kinematics in the Larderello geothermal area (Italy): Insights for the interpretation of the present stress field," *Geothermics*, vol. 83, no. September 2019, p. 101714, 2020, doi: 10.1016/j.geothermics.2019.101714.
- [4] B. Tauzin, T. S. Pham, and H. Tkalčić, "Receiver functions from seismic interferometry: A practical guide," *Geophys. J. Int.*, vol. 217, no. 1, pp. 1–24, 2019, doi: 10.1093/gji/ggz002.
- [5] G. Kaviris, I. Spingos, V. Karakostas, E. Papadimitriou, and T. Tsapanos, "Shear-wave splitting properties of the upper crust, during the 2013–2014 seismic crisis, in the CO₂-rich field of Florina Basin, Greece," *Phys. Earth Planet. Inter.*, vol. 303, no. March, p. 106503, 2020, doi: 10.1016/j.pepi.2020.106503.
- [6] I. Spingos, G. Kaviris, C. Millas, P. Papadimitriou, and N. Voulgaris, "Pytheas: An open-source software solution for local shear-wave splitting studies," *Comput. Geosci.*, vol. 134, no. 104346, 2020, doi: 10.1016/j.cageo.2019.104346.
- [7] W. Diningrat, S. R. A. Sugiono, and Y. Daud, "Fault-related fractures characteristic of Kijang fault at Wayang Windu Geothermal field," *IOP Conf. Ser. Earth Environ. Sci.*, vol. 254, no. 1, 2019, doi: 10.1088/1755-1315/254/1/012007.
- [8] L. M. Kenyon and I. Wada, "Mantle Wedge Seismic Anisotropy and Shear Wave Splitting: Effects of Oblique Subduction," *J. Geophys. Res. Solid Earth*, vol. 127, no. 4, pp. 1–18, 2022, doi: 10.1029/2021JB022752.
- [9] G. Kaviris, I. Spingos, V. Kapetanidis, and C. Millas, "An upper crust shear-wave splitting in Attica (Central Greece) based on recordings of the 1999 and 2018 earthquake sequences An upper crust shear-wave splitting in Attica (Central Greece) based on recordings of the 1999 and 2018 earthquake sequences," in *3rd European Conference on Earthquake Engineering & Seismology*, 2022, no. October, pp. 3547–3554.
- [10] S. Crampin, "Shear-wave splitting: New geophysics and earthquake stress-forecasting," *Encycl. Earth Sci. Ser.*, vol. Part 5, pp. 1355–1365, 2011, doi: 10.1007/978-90-481-8702-7_19.
- [11] J. M. Dubé, F. A. Darbyshire, M. V. Liddell, R. Stephenson, and G. Oakey, "Seismic anisotropy of the Canadian High Arctic: Evidence from shear-wave splitting," *Tectonophysics*, vol. 789, no. November 2019, p. 228524, 2020, doi: 10.1016/j.tecto.2020.228524.
- [12] Y. Gao, A. Chen, Y. Shi, Z. Zhang, and L. Liu, "Preliminary analysis of crustal shear-wave splitting in the Sanjiang lateral collision zone of the southeast margin of the Tibetan Plateau and its tectonic implications," *Geophys. Prospect.*, vol. 67, no. 9, pp. 2432–2449, 2019, doi: 10.1111/1365-2478.12870.
- [13] Y. Gao, J. Wu, Y. Fukao, Y. Shi, and A. Zhu, "Shear wave splitting in the crust in North China: Stress, faults and tectonic implications," *Geophys. J. Int.*, vol. 187, no. 2, pp. 642–654, 2011, doi: 10.1111/j.1365-246X.2011.05200.x.
- [14] A. M. McPherson, D. H. Christensen, G. A. Abers, and C. Tape, "Shear Wave Splitting and Mantle Flow Beneath Alaska," *J. Geophys. Res. Solid Earth*, vol. 125, no. 4, pp. 1–18, 2020, doi: 10.1029/2019JB018329.
- [15] W. Utama, D. Desa, and S. Ardhya, "Identification of Micro-Earthquake Hypocenters using Geiger and Coupled Velocity-Hypocenters Methods," *Int. J. Adv. Sci. Eng. Inf. Technol.*, vol. 11, no. 1, pp. 350–355, 2021.
- [16] Z. Zhang, J. A. Fleurisson, and F. L. Pellet, "A case study of site effects on seismic ground motions at Xishan Park ridge in Zigong, Sichuan, China," *Eng. Geol.*, vol. 243, no. June, pp. 308–319, 2018, doi: 10.1016/j.enggeo.2018.07.004.
- [17] I. Hanif, A. Zaenudin, Rustadi, N. Haerudin, and R. C. Wibowo, "Identifikasi Orientasi Rekahan Mikro Area Panas Bumi Monte Amiata Berdasarkan Analisis Studi Shear Wave Splitting," *Indones. Phys. Rev.*, vol. 3, no. 2, pp. 3–5, 2020.
- [18] S. M. Mousavi, W. L. Ellsworth, W. Zhu, L. Y. Chuang, and G. C. Beroza, "Earthquake transformer—an attentive deep-learning model for simultaneous earthquake detection and phase picking," *Nat. Commun.*, vol. 11, no. 1, pp. 1–12, 2020, doi: 10.1038/s41467-020-17591-w.
- [19] A. Vizzaccaro, A. Opreni, L. Salles, A. Frangi, and C. Touzé, "High order direct parametrisation of invariant manifolds for model order reduction of finite element structures: application to large amplitude vibrations and uncovering of a folding point," *Nonlinear Dyn.*, vol. 110, no. 1, pp. 525–571, 2022, doi: 10.1007/s11071-022-07651-9.
- [20] A. Mihaylov, H. El Naggat, D. Mihaylov, and S. Dineva, "Approximate analytical HVSR curve using multiple band-pass filters and potential applications," *Soil Dyn. Earthq. Eng.*, vol. 127, no. June, p. 105840, 2019, doi: 10.1016/j.soildyn.2019.105840.
- [21] J. P. Métaixian *et al.*, "Migration of seismic activity associated with phreatic eruption at Merapi volcano, Indonesia," *J. Volcanol. Geotherm. Res.*, vol. 396, p. 106795, 2020, doi: 10.1016/j.jvolgeores.2020.106795.
- [22] A. Scala *et al.*, "Monitoring the Microseismicity through a Dense Seismic Array and a Similarity Search Detection Technique: Application to the Seismic Monitoring of Collalto Gas-Storage, North Italy," *Energies*, vol. 15, no. 3504, 2022, doi: 10.3390/en15103504.
- [23] C. Yi, H. Wang, L. Ran, L. Zhou, and J. Lin, "Power spectral density-guided variational mode decomposition for the compound fault diagnosis of rolling bearings," *Meas. J. Int. Meas. Confed.*, vol. 199, no. April, p. 111494, 2022, doi: 10.1016/j.measurement.2022.111494.
- [24] D. Naidoo and V. M. Srivastava, "Third Order Band Pass Filter With Double-Gate MOSFET: A Simulation Perspective," *IOP Conf. Ser. Mater. Sci. Eng.*, vol. 1126, no. 1, p. 012019, 2021, doi: 10.1088/1757-899x/1126/1/012019.
- [25] A. Yadav, M. K. Dutta, and J. Prinosil, "Machine Learning Based Automatic Classification of Respiratory Signals using Wavelet Transform," *43rd Int. Conf. Telecommun. Signal Process. TSP 2020*, pp. 545–549, 2020, doi: 10.1109/TSP49548.2020.9163565.
- [26] S. Petrosino and L. De Siena, "Fluid migrations and volcanic earthquakes from depolarized ambient noise," *Nat. Commun.*, vol. 12, no. 1, pp. 1–8, 2021, doi: 10.1038/s41467-021-26954-w.
- [27] J. Baron, I. Primofiore, P. Klin, G. Vessia, and G. Laurenzano, *Investigation of topographic site effects using 3D waveform modelling: amplification, polarization and torsional motions in the case study of Arquata del Tronto (Italy)*, vol. 20, no. 2. Springer Netherlands, 2022.
- [28] Y. Li, D. Li, L. Huang, Y. Zheng, P. Wannamaker, and J. Moore, "Anisotropic properties in the sedimentary and granite rocks at the Utah FORGE geothermal site revealed by shear-wave splitting of 3-component borehole microseismic data," in *2nd International Meeting for Applied Geoscience & energy*, 2022, pp. 3619–3623, doi: 10.1190/image2022-3750065.1.

- [29] J. Asplet, J. Wookey, and M. Kendall, "A potential post-perovskite province in D" beneath the Eastern Pacific: Evidence from new analysis of discrepant SKSa-SKKS shear-wave splitting," *Geophys. J. Int.*, vol. 221, no. 3, pp. 2075–2090, 2020, doi: 10.1093/GJI/GGAA114.
- [30] B. A. Brooks *et al.*, "Robust Earthquake Early Warning at a Fraction of the Cost: ASTUTI Costa Rica," *AGU Adv.*, vol. 2, no. 3, pp. 1–17, 2021, doi: 10.1029/2021av000407.
- [31] E. M. Nathan, A. Hariharan, D. Florez, and K. M. Fischer, "Multi-Layer Seismic Anisotropy Beneath Greenland," *Geochemistry, Geophys. Geosystems*, vol. 22, no. 5, pp. 1–17, 2021, doi: 10.1029/2020GC009512.
- [32] Z. Wang, X. Li, and X. Shang, "Distribution Characteristics of Mining-Induced Seismicity Revealed by 3-D Ray-Tracing Relocation and the FCM Clustering Method," *Rock Mech. Rock Eng.*, vol. 52, no. 1, pp. 183–197, 2019, doi: 10.1007/s00603-018-1585-z.
- [33] R. Kumari, P. Kumar, N. Kumar, and Sandeep, "Role of site effect for the evaluation of attenuation characteristics of P, S and coda waves in Kinnaur region, NW Himalaya," *J. Earth Syst. Sci.*, vol. 129, no. 1, 2020, doi: 10.1007/s12040-020-01454-5.